Earth And Planetary Science Letters
June 2019, Volume 516 Pages 108-121
https://doi.org/10.1016/j.epsl.2019.04.004
https://archimer.ifremer.fr/doc/00773/88514/

Melt hybridization and metasomatism triggered by syn-magmatic faults within the Oman ophiolite: A clue to understand the genesis of the dunitic mantle-crust transition zone

Rospabé Mathieu [1, 2, *], Benoit Mathieu [1], Ceuleneer Georges [1], Kaczmarek Mary-Alix [1], Hodel Florent [1]

[1] Univ Toulouse, CNRS, IRD, Observ Midi Pyrenees,GET, 14 Ave E Belin, F-31400 Toulouse, France.
[2] Japan Agcy Marine Earth Sci & Technol JAMSTEC, Res Inst Marine Geodynam IMG, 2-15 Natsushima, Yokosuka, Kanagawa 2370061, Japan.

* Corresponding author : Mathieu Rospabé, email address : mathieu.rospabe@get.omp.eu

Abstract :

On Earth, most of the critical processes happen at the frontiers between envelopes and especially at the Moho between the mantle and the crust. Beneath oceanic spreading centers, the dunitic transition zone (DTZ) appears as a major interface between the upwelling and partially molten peridotitic mantle and the accreting gabbroic lower crust. Better constraints on the processes taking part in the DTZ allows improved understanding of the interactions between silicate melts and hydrated fluids, which act competitively to generate the petrological Moho. Here we combine mineral and whole rock major and trace element data with a structural approach along three cross-sections up to 300 m thick above the fossil Maqsad mantle diapir (Oman ophiolite) in order to understand the vertical organization of the DTZ with depth. Our results highlight that most of the faults or fractures cross-cutting the DTZ were ridge-related and active at an early, high temperature magmatic stage. Chemical variations along the cross-sections define trends with a characteristic vertical scale of few tens of meters. There is a clear correlation between the chemical variation pattern and the distribution of fault zones, not only for fluid-mobile elements but also for immobile elements such as REE and HFSE. Faults, despite displaying very limited displacements, enhanced both melt migration and extraction up to the crust and deep hydrothermal fluids introduction down to the Moho level. We propose that these faults are a vector for upwelling melt modification by hybridization, with hydrothermal fluids and/or silicic hydrous melts, and crystallization. Infiltration of these melts or fluids in the country rock governs part of the gradational evolutions recorded in composition of both the olivine matrix and interstitial phases away from faults. Finally, these faults likely control the thermal structure of the mantle-crust transition as evidenced by the spatial distribution of the crystallization products from percolating melts, organizing the transition zone into pure dunites to impregnated dunites horizons. In this context, the DTZ appears as a reactive interface that developed by the combination of three primary processes: tectonics, magmatism and deep, high temperature hydrothermal circulations. Accordingly, these features fundamentally contribute to the variable petrological and geochemical organization of the DTZ and possibly of the lower crust below oceanic spreading centers, and may be a clue to interpret part the heterogeneity observed in MORB signatures worldwide.

Highlights

► The dunitic transition zone in the Oman ophiolite shows vertical chemical evolutions. ► Syn-magmatic faults cut across the DTZ and influence chemical variations. ► Melt-fluid-rock reactions within the DTZ are strongly controlled by faults.

Keywords : Oman ophiolite, dunitic mantle-crust transition zone, syn-magmatic faulting, melt-rock reactions, high temperature hydrothermalism, melt hybridization

1. Introduction

The oceanic crust is generated at spreading centers where extensive thermal and chemical exchanges occur between the mantle, the crust and the external envelopes. Crustal accretion at oceanic spreading centres is not a steady state process, proceeding by the cyclic succession of magmatic and magma-starved episodes, whatever the spreading rate (e.g. Gente et al., 1995; Sinton et al., 2002; Yeo et al., 2016). During periods of magmatic quiescence, the front of hydrothermal systems can deepen significantly, a propagation likely triggered by normal faulting and detachment faults. This leads to the efficient cooling and alteration of the mafic-ultramafic substratum and to elements mobilization and redistribution (e.g. German et al., 2016 among recent studies), and therefore impacts chemical exchanges happening along oceanic spreading centers. In addition, there is accumulating evidence for magmatism-hydrothermalism relationships beneath oceanic spreading centres, in temperature conditions high enough to induce the re-melting of previously hydrated rocks (e.g. Amri et al, 1996; Benoit et al, 1999; Koepke et al., 2005; Zhang et al., 2017 and references therein) or allowing crystallizing magmas and hydrothermal fluids to interact (e.g. Abily et al., 2011; Rospabé et al., 2017). The Oman ophiolite has been shown to be an excellent analogue of present-day spreading centres to study deep-seated hydrothermal processes, whatever its precise tectonic setting (i.e. Mid-Ocean Ridge vs. arc-related basin) (e.g. Bosch et al., 2004; Currin et al., 2018; France et al., 2009, 2013; Gilgen et al., 2016; Python et al., 2007; Zihlmann et al., 2018).

In the Oman ophiolite, petrological and isotopic studies have shown that the crust was affected by hydrothermal circulations ranging from greenschist to upper amphibolite/granulite facies (e.g. Bosch et al., 2004; Gregory and Taylor, 1981; Koepke et al., 2005; Nehlig and Juteau, 1988; Currin et al., 2018). The formation of diopsidite and rodingite dikes likewise involves high temperature hydrothermal fluids circulating down to the Moho and even below (Akizawa et al., 2011; Python et al., 2007). Most of these alteration features post-date the crystallization stage and are introduced at depth via fracture networks (Nehlig and Juteau, 1988; Reuber, 1988). However, when normal faults develop early and root at Moho level, seawater can locally reach the incompletely crystallized lower crust (Abily et al., 2011).

The dunitic transition zone (DTZ) from the Maqsad area (Oman ophiolite), like dunites from other ophiolites (e.g. Quick, 1981; Ceuleneer and Le Sueur, 2008; Sanfilippo et al., 2014; 2017), displays extensive petrological and geochemical variations that result from the overprint of several magmatic processes: incongruent melting of harzburgite orthopyroxenes (i.e. "dunitization"), chemical re-equilibration between the olivine matrix and percolating melts, refertilization by variably evolved melt batches (Rospabé et al, 2018a). In addition to interstitial plagioclase and clinopyroxene reflecting the fractionation from a percolating MORB (Abily and Ceuleneer, 2013; Koga et al., 2001), the occurrence of orthopyroxene, amphibole, diopside and garnet, both in interstitial position and - with mica - included in chromite, highlights the early contribution of a more exotic, hydrated and silica-richer component that variably mixed with the MORB (Rospabé et al., 2017). The composition and bottom to top distribution of minerals that crystallized in response to this hybridization process calls for a hydrothermal origin of the water rather than a deep, subduction-related origin. Chromitites associated to minerals of high temperature hydrothermal origin are ubiquitous at Moho level in the Oman ophiolite. Accordingly, if can be inferred that this process affected the whole ophiolite. However, the way in which this hydrated component was introduced at high temperature within the DTZ remains poorly constrained. In order (1) to specify the petrological, geochemical and tectonic structuration of the DTZ beneath oceanic spreading centres and (2) to decipher the enigmatic relationships between the tectonic history of the DTZ and its imbricated magmatic and hydrothermal signatures, we investigated a portion of the paleo-ridge axis related to the Maqsad mantle diapir. This area appears densely faulted according to previous geological maps (Amri, 1995; Rabu et al., 1986). Our results highlight that faults were active early at Moho level, since the magmatic stage, and that they conditioned the petrological and geochemical organization of the DTZ, and probably of the overlying lower crust, by exerting a strong control on the mantle harzburgite dunitization and on melts migration and crystallization.

2. Geological setting

2.1. Geology of the Oman ophiolite

The Oman ophiolite is the largest (~500 × 50 km) remaining oceanic lithosphere fragment from the Tethyan ocean. It formed along a (possibly fast) spreading ridge ~95-97 million years ago (e.g. Boudier et al., 1988; Rioux et al., 2013 and references therein). The synoptic mapping of plastic deformation structures preserved in mantle peridotites allowed characterizing vertical flow patterns in several areas; they were interpreted as upwelling asthenospheric diapirs beneath the former oceanic ridge axis along which the lithosphere accreted (Ceuleneer et al., 1988; Jousselin et al., 1998; Nicolas et al., 1988). The paleo-ridge axis orientation evolves from a N-S direction in the north of the ophiolite to NW-SE in the south, although exceptions to this general tendency can be observed locally (e.g. MacLeod and Rothery, 1992; Nicolas et al., 1988; Pallister, 1981). The mapping of the nature of the dikes cropping out within the mantle section (Python and Ceuleneer, 2003) has evidenced a MORB-like environment mainly in the SE massifs of the ophiolite, together with other restricted occurrences, while a depleted calc-alkaline magmatism is observed elsewhere.

2.2. The Sumail Massif

The Sumail massif, located in the SE of the ophiolite and focus of the present study, exposes the well preserved Maqsad fossil mantle diapir and its associated N130 trending paleo-spreading centre (Ceuleneer, 1991; Ceuleneer et al., 1988; Jousselin et al., 1998) (Fig. 1A). It fed the largest (~80 × ~30 km) MORB area of the Oman ophiolite (Python and Ceuleneer, 2003). The intense igneous activity related to the diapir is witnessed by abundant melt migration structures cropping out in mantle harzburgites (Benoit et al., 1996; Ceuleneer et al., 1996; Python and Ceuleneer, 2003), by the 300-400 m thick DTZ in between mantle and crustal sequences (Abily and Ceuleneer, 2013; Boudier and Nicolas, 1995; Ceuleneer and Nicolas, 1985; Jousselin et al., 1998; Rospabé, 2018), and by abundant chromitite ore bodies (Ceuleneer and Nicolas, 1985). The Sumail massif was slightly tilted by post-accretion tectonism, its regional dip does not exceed 10° to the SE.

Two sets of highly dipping faults confer to the Maqsad area its more salient tectonic and morphologic features according to geological maps (Amri, 1995; Rabu et al., 1986): (1) One strikes N130 and is parallel to the strike of the sheeted dike complex in this area, i.e. parallel to the regional orientation of the inferred paleo-ridge axis (Ceuleneer, 1991; MacLeod and Rothery, 1992; Pallister, 1981) (Fig. 1A). This system may reasonably be related to the former spreading activity since it has been evidenced that N130-trending faults have generally a normal offset and have locally disturbed crystallization sequences in the lowermost gabbroic crust in this area, in association with hydrothermal fluids (Abily et al., 2011). N130 is also the azimuth of the olivine gabbro dykes in the mantle section of the Maqsad area (Ceuleneer et al, 1996). (2) The other fault system strikes N160 to N-S, parallel to the Muqbariah high temperature mylonitic shear zone (Amri et al., 1996; Ceuleneer, 1991) (Fig. 1A). Moving away from the diapir, the diverging mantle flow is limited to the SW by the Muqbariah shear zone, itself injected by numerous dikes from a depleted andesite kindred, contrasting with the MORB signature of the dykes present in the diapir and at its immediate periphery, and to the NE by an area injected by pegmatitic dikes and intrusions from the same andesitic melts (Amri, 1995; Amri et al., 1996; Benoit et al., 1999). It has been proposed on the basis of geological and isotopic arguments that these intrusions and dykes originated from "lithospheric" melts generated by the remelting of hydrothermally altered peridotites at an early stage of interaction between the lithosphere and the rising Maqsad diapir (Amri et al., 1996; Benoit et al., 1999; Clénet et al., 2010). Although no detailed study was conducted yet about the interplay between SW-NE spreading and shearing along N160-180 shear zones, first evidence show they took place early during the Maqsad ridge development.

3. Organization of the DTZ along the Maqsad paleo-ridge axis

We report here below on the structural, petrological and geochemical characteristics of three cross-sections sampled through the Maqsad DTZ. These sections were selected among twenty we explored in this area (Rospabé, 2018) because they particularly well illustrate the interactions between early faulting and geochemical evolution of the DTZ. They were collected along the inferred paleo-ridge axis northwest to the centre of the fossil diapir (Fig. 1A), with from north to south the sections #1, #2 and #3 (Fig. 1B, Supplementary Table S1). The sampling was performed in a W-E orientation from the wadi Mahram to the west (altitude ~635 m) to the top of the DTZ to the east, exposed at an altitude of ~1070 m in this area (Fig. 1B). The sampling interval ranges from 10 to 20 m vertically. We adopted this strategy in order to cross the two N130 and N165-180 trending fault systems cross-cutting the DTZ. Chemical evolutions along the DTZ are presented for mineral and whole rock major elements as well as for whole rock trace elements for a total of 125 samples. Mineral and whole rock compositions are given in Supplementary Table S2 and Supplementary Table S3 respectively. Analytical methods are detailed in the Electronic Supplement 1.

3.1. Tectonic structuration of the DTZ

3.1.1. The N130 fault system

The N130 faults are regularly spaced by horizontal distances of ~250 meters on average. They can be followed along strike on up to 2 km and have generally a dip of 65-70° toward the NE. The cross-section #2 exposes conversely two successive faults with a dip toward the SW (Fig. 1B). The amplitude of the displacement along N130 faults has been established in a few cases where they offset plurimetric troctolites intrusions: the movement is normal and the displacement is limited to a few meters at most. A troctolite lens located about 1.5 km westward of the considered cross-sections developed a strong high temperature deformation along a N130.70NE normal fault (Fig. 2A), similarly to what was described at the base of the crustal section near Maqsad (Abily et al., 2011). The N130 fault zones display clear brittle features near the top of the DTZ and appear to be progressively rooted through the DTZ where they evolve to serpentine and carbonate breccias. Brecciated zones reach up to about 10 meters in thickness concerning major faults. The alteration halo having affected the dunitic wall rock does not exceed a few meters.

3.1.2. The N165-180 fault system

The N165-180 system accommodated a transtensional movement with a clear normal and more subtle dextral components. This system is represented by two main discontinuities in the explored area, the western N165-180-trending one making the contact between the mantle section and the DTZ, and the easternmost ~N165 being internal to the DTZ (Fig. 1B):

- The westernmost N165-180 major discontinuity is organized as an asymmetric graben-type structure limited by two N165.85E to vertical and N180.80W faults (Fig. 1B). It induced the collapse of a layered troctolite unit down to the base of the DTZ, supporting a significant normal movement. This system clearly evolved during a long time scale, starting with early, syn- to sub-magmatic deformations - gabbros boudins, elongated mafic intrusions (Fig. 2B) -, and becoming progressively affected by increasingly brittle fracturing as well as by greenschist facies alteration of surrounding rocks. The schistosity within the N165.85E fault centre, making the contact between mantle harzburgites and DTZ dunites (Fig. 1B), points to an intense dextral movement similar to the dominant motion recorded by the Muqbariah mylonitic shear zone (Amri et al., 1996).

- The second system affecting the DTZ internally evolves from a N155.65NE direction to the south, along the cross-section #3, to a N170 sub-vertical orientation to the north along the two cross-sections #1 and #2 (Fig 1B). It accommodated a transtensional movement with a normal displacement much lower than along the westernmost system in regard to the absence of deformation in its centre. The strike-slip along this discontinuity is estimated to about 80 m at most regarding two N130 fault segments offset, with a dextral movement, north to the cross-section #1. Likewise, the geological map from Rabu et al. (1986) generally shows N130 faults cross-cut and shifted by the later N165 system. However, we also observed the reverse relationships in some locations with the disruption of N165-180 factures by later N130 faults, pointing out the contemporaneity of both systems.

Other minor N165-180 faults or fractures affecting the DTZ, few meters in width at most, become more abundant upsection. They confer a shale-like parting to the dunites while examination of thin section reveals no evidence of high-temperature mylonitic deformation (Fig. 2C). Shear sense indicators are poorly developed and vertical offsets seem to be restricted to a few meters, making of these fractures transtensional to purely extensional cracks. They are mostly subvertical or with a strong dipping generally to the west. Along these fractures, troctolite intrusions are affected by greenschist facies metamorphism while serpentine and carbonate developed into or parallel to the fracture plans in surrounding dunites. Along a companion N165.80W fault right to the west of the easternmost major discontinuity, a swarm of undeformed gabbro dikes oriented according to both N125.70NE and N105.60NE orientations cuts across the N165-trending schistosity, stressing on the early fault development before melt percolation and fluids circulation and subsequent alteration (Fig. 2C).

3.2. Petrological sequences within the DTZ

Previous studies described a highly variable mineralogical content within the Maqsad DTZ, with dunites evolving from "pure", containing only olivine together with a few percent of scattered chromite grains and rare, small clinopyroxene, to strongly impregnated (up to 30% of interstitial minerals) (e.g. Abily and Ceuleneer, 2013; Boudier and Nicolas, 1995; Koga et al., 2001). Impregnated dunites contain one or more interstitial mineral phases among clinopyroxene, plagioclase, orthopyroxene, amphibole and other accessory minerals (e.g. hydrothermal diopside, grossular garnet) (Rospabé et al., 2017). Hence, dunites from the Maqsad DTZ are classified in the present study as pure dunites, cpx-bearing dunites, pl/cpx-bearing dunites, opx/pl/cpx-bearing dunites and amph-bearing dunites (± opx/pl/cpx) (Rospabé et al., 2018a).

The contacts between the main units composing the ophiolite are frequently faulted within the studied area. Mantle harzburgites were not observed along the wadi Mahram except to the west of the major westernmost N165 tectonic accident (Fig. 1B). The three sampled cross-sections are entirely made of variably impregnated dunites and contain a high abundance of troctolite intrusions upsection (Fig. 3). These intrusions, plurimetric in size and cumulative in texture, display clear intrusive relationships at the contact with surrounding dunites showing they were injected within the near-solidified DTZ. The cross-sections #1 and #3 present a similar lithological succession, with a lower half part made of pure dunites and an upper part widely impregnated. The transition from pure to impregnated portions corresponds to the major easternmost ~N165 discontinuity. The pure dunitic lower units regularly contain small size (100 µm at most) clinopyroxene or hybrid diopside (i.e. hybrid between igneous clinopyroxene and hydrothermal diopside; Rospabé et al., 2017) in interstitial position along olivine grain boundaries (Fig. 4A). We observed locally, approaching fault zones, a higher amount of chromite, occurring as schlierens and more rarely as massive dikes (Fig. 4B). Along the cross-section #1, clinopyroxene and a scarce amount of plagioclase progressively appear just above the major eastern N170 fault (Fig. 3). They become much more abundant together with the appearance of orthopyroxene and amphibole twenty meters above, in the uppermost section part, beyond a N130.60NE fault. Along the cross-section #3, clinopyroxene, plagioclase, orthopyroxene and amphibole appear all together above the N155 segment, directly in the southward continuity of the eastern ~N165 major discontinuity (Fig. 3). These mineral phases are observed all along the impregnated upper part. Plagioclase is slightly more abundant than clinopyroxene until a N175 fault zone, while clinopyroxene and orthopyroxene are more frequently observed above (Fig. 4C). Amphibole is unequally distributed along the section.

The cross-section #2, located midway from sections #1 and #3, does not respect this dichotomous structuration (Fig. 3). Interstitial amphibole, plagioclase and clinopyroxene are more frequent all along this section (Figs. 4D and E) while pure dunites are quite uncommon. Despite this erratic mineral distribution, amphibole appears more abundant in specific subsections, limited by both N130 and N165-N180 faults zones, while orthopyroxene is restricted to the uppermost level above a N130.55SW fault.

3.3. DTZ geochemical patterns

The olivine chemical content is highly variable in dunites collected along the Maqsad DTZ, with Fo and NiO contents varying from 93.2 to 85.7 and from 0.16 to 0.45 wt.% respectively.

The olivine composition does not correlate with the presence/abundance of other minerals (Fig. 5A).

Pure dunites are characterized by U- or V-shaped REE patterns (La_{CN}/Sm_{CN} = 0.60-3.8; Gd_{CN}/Yb_{CN} = 0.05-0.27) and by enrichment in LILE and positive Pb, Sr and Ti anomalies in regard to REE in their extended trace element patterns (Fig. 6B). Impregnated samples containing clinopyroxene, plagioclase, orthopyroxene and/or amphibole interstitially between olivine grains generally show convex-upward REE patterns characterized by HREE to LREE depletion (La_{CN}/Yb_{CN} = 0.02-0.42) (Fig. 6B).

Mineral and whole rock compositions as a function of the sampling altitude are shown in figures 6 and 7 (see also the Electronic Supplement 2). The regional N130 and N165-180 faults are reported at the altitude they cut across each section respectively (see Figure 3 for their dipping). Chemical variations are not randomly distributed from one sampling point to another: they display progressive and successive increasing or decreasing evolutions (depending on the regarded element) with inversions from a trend to another every hundred meters approximately. In the following we propose to show how the different chemical trends are related (1) to the samples modal composition, (2) to their position relative to fault zones, or (3) if they are essentially cryptic (i.e. unrelated to lithological or structural features).

3.3.1. Chemical trends related to lithological facies

Mineral and whole rock chemical compositions are highly variable in the Maqsad DTZ dunites (Rospabé et al., 2018a). Whole rock vertical composition evolutions are partly controlled by the modal composition of the samples. High amount of interstitial phases (essentially plagioclase and pyroxene), likely related to impregnation (Fig. 4), leads to an increase in CaO and Li contents, in the Gd_{CN}/Yb_{CN} ratio and the concavity of REE patterns ($\sqrt{(Sm_{CN} \times Gd_{CN})}/\sqrt{(Ce_{CN} \times Yb_{CN})}$ -1), and to a decrease in La_{CN}/Sm_{CN} and Nb/Ta ratios (Fig.

7 and Electronic Supplement 2). The Cr content directly reflects the few percent of disseminated chromite in dunites, which also seems to control the whole rock Zr/Hf ratio (Electronic Supplement 2).

The most impressive mineral composition variations along the three cross-sections are observed in pure dunites or more generally at the base of each section below the N155-170 fault (Fig. 6). They are unpredictable as they are not related to the samples modal composition. Conversely, Fo in olivine (100 × molar $Mg/(Mg + Fe_{total})$), XCr in chromite (100 × molar Cr/(Cr + Al)) (Fig. 6) and Mg# in whole rock (100 × molar $Mg/(Mg + Fe_{total})$) (Fig. 7) are much less variable in impregnated dunites, whatever the nature of interstitial minerals.

3.3.2. Chemical trends related to fault zones

In some cases, especially in pure dunites, the vertical evolution of chemical signatures along the cross-sections define patterns that appear to be influenced by the distribution of major fault zones, whatever their orientation. In details, the Fo in olivine, XCr in chromite and Mg# in whole rock decrease down to values of about 88 or below, ~45 and ~87 respectively approaching faults (e.g. the interval ~700-725 m in the three sections; Figs. 5 and 6). NiO in olivine and Ni in whole rock follow the same tendency as well as the Mg# (100 × molar $Mg/(Mg + Fe^{2+})$) in clinopyroxene, orthopyroxene and amphibole, both when they are interstitial between olivine grains or as inclusions in chromite (Electronic Supplement 2). The La_{CN}/Sm_{CN} and U/Th ratios in pure dunites also decrease until 1 and below 0.75 respectively (toward 700 m and 775 m in altitude in the cross-section #1, 725 m and 850 m in the cross-section #3; Fig. 7). These variations are correlated with an increase of the CaO content in olivine in pure dunites (until ~0.3 wt.%), TiO_2 content in pyroxenes (up to 0.5 wt.%) (Fig. 6

and Electronic Supplement 2). Similarly, Gd_{CN}/Yb_{CN} (and thus the concavity of the REE patterns) and Nb/Ta ratios in whole rocks increase in pure dunites toward most of the fault zones (Fig. 7 and Electronic Supplement 2).

3.3.3. Chemical trends unrelated to lithological or structural features

Beyond variations related to the amount of interstitial phases (local-scale) or approaching fault zones (tens of meter-scale), we can observe chemical evolutions depending on the altitude along the whole DTZ. In this frame, Mg# and Ni content in both whole rock and minerals generally decrease in the uppermost part of the DTZ. In the same time TiO_2 content in ortho- and clinopyroxene and Na_2O content in amphibole increase whatever their mode of occurrence (i.e. interstitial between olivine grains or included in chromite). This suggests that DTZ dunites recorded the cumulate effect of several processes involved in their formation. Concerning few chemical proxies, such as Co in whole rock or YFe^{3+} in chromite, their vertical evolution is partly correlated to the presence of fault zones but without clear systematic increasing or decreasing trend (Electronic Supplement 2). This leads to the alternation of positive and negative correlations between Ni and Co in some horizons like at the base of the cross-section #1.

3.3.4. Focus on clinopyroxene major element zoning

It was shown in previous studies that chemical zonings in interstitial minerals in deeply impregnated mantle-derived rocks probably reflect melt/rock reactions (e.g. Drouin et al., 2009; Sanfilippo et al., 2015). Among the studied impregnated samples, twenty chemical profiles were performed across single grains of clinopyroxene in order to investigate the pattern of possible zoning in their major element composition as it was already reported (even if not systematic) in some cases (Koga et al., 2001; Rospabé et al., 2018a). This was made for clinopyroxene of various sizes in 11 samples displaying various interstitial minerals in variable amount. Half of the analyzed clinopyroxene shows an increase in Mg# (up to 92.5), and in SiO_2 and TiO_2 contents (up to 53.8 wt.% and 0.33 wt.% respectively), associated to a decrease of Al_2O_3 and Cr_2O_3 contents (down to 2.8 wt.% and 1.2 wt.% respectively), from core to rims (Fig. 8A). The other half does not show zoning in Mg# and SiO_2, and show normal zoning in Al_2O_3 and Cr_2O_3 in some cases only (Fig. 8B). It appears that both the chemical content of and the presence/absence of zoning in clinopyroxene are independent of the paragenetic assemblage, neither with the degree of impregnation nor with the size of the considered clinopyroxene crystal. However, well-defined zonings are systematically observed in samples collected close to fault zones. Oppositely, chemically weakly zoned clinopyroxenes are observed in samples located everywhere in the DTZ, independently from any fault location.

4. Interpretations and discussion

4.1. Early syn-magmatic faulting at Moho level

The faults located between the distinctive main units of the Sumail massif were originally attributed to later tectonic events postdating the oceanic lithosphere accretion, potentially related to the emplacement of the ophiolitic nappe onto the Arabian margin (Amri, 1995; Glennie et al., 1974; Rabu et al., 1986). Other studies interpreted the development of the both N130 and N165 tectonic systems as synchronous with magmatism, these features being responsible for the deformation and disturbed crystallization in the lower crustal, layered gabbros along N130 faults (Abily et al., 2011; Jousselin et al., 1998), and of the genesis of plagiogranitic and andesitic intrusions within the N165-trending Muqbariah regional shear zone system (Amri et al., 1996; Benoit et al., 1999).

We observed that the DTZ was also affected by the both N130 and N165-180 systems (Fig. 1B), which led to a stronger serpentinization and carbonation of surrounding dunites. In spite of these ubiquitous witnesses of low temperature hydrothermal circulations, some outcrops preserved strong evidence of a high temperature deformation of the magmatic products along the both fault systems (Figs. 2A and B). Excepting the two main N165-180 discontinuities, which accommodated a significant strike-slip displacement (i.e. estimated to 80 m horizontally concerning the easternmost one), other faults are better described as cracks with a movement restricted to a few meters at most. The N130-trending faults may reasonably be related to the ridge accretion, the strike of the sheeted dike complex displaying the same orientation in this area (MacLeod and Rothery, 1992; Pallister, 1981). The slight normal displacement on fault planes, generally measured with a dip of 50 to 70° at a regional scale, locally induced the syn-magmatic deformation and the disturbance of crystallization sequences in layered troctolites and gabbros at the transition between the crustal section and the DTZ (Fig. 2A; see also Abily and Ceuleneer, 2011). The two areas affected by N130 faults with an opposite dipping toward the SW (along the cross-section #2) define local graben-type structures accommodating the general extensional frame (Fig. 1B). We observed that N130 oriented mafic dikes, viewed as cumulates after the last basaltic melt batches discharged from the Maqsad diapir (Ceuleneer et al., 1996), cut across the tectonic lineaments, especially the transtensional N165 ones (Fig. 2C). This supports that most of the N130 and N165 tectonic events on one hand and the magmatic activity on the other hand developed then ceased contemporaneously.

Otherwise, chemical variations observed vertically along the DTZ constitute an independent and indirect argument supporting syn-magmatic fluid circulation along faults that experienced moderate displacement. The minerals (both olivine and impregnating phases) and bulk-rock display evolutions of their composition over tens of meters vertically toward the fault zones, including for immobile elements or element ratios, expected to be related to magmatic processes only (e.g. XCr in chromite, TiO_2 in impregnant minerals or REE and HFSE in bulk-samples; Figs. 5 and 6, Electronic Supplement 2). Such continuous evolutions suggest that faults played an important role in the DTZ genesis and are consistent with a moderate amplitude of the displacements along fault planes: major offsets post-dating the DTZ formation would have partly erased the systematic chemical trends observed approaching the faults. It is worth mentioning that common vertical chemical evolutions are observed both in minerals composing dunites as well as in silicate inclusions, supposed to be isolated early by their host chromite. Consequently, all these observations allow us to interpret both N130 and N165 oriented faults as structures developed early at a high temperature, syn-magmatic stage. They strongly influenced the petrological and geochemical organization of the DTZ, although they continued to be main vectors for hydrothermal fluids at lower temperature, following the cessation of any magmatic activity.

4.2. Relationships between faulting and melt-rock reactions

4.2.1. Faulting and percolating melts characteristics

The relationship between fault zones and minerals/whole rock compositions designs several similar chemical evolutions along the three cross-sections - especially between cross-sections #1 and #3 that also display a similar petrological sequence (Fig. 3). Fault zones partly condition the chemical patterns recorded in the dunitic matrix as revealed by olivine and pure dunites whole rock compositions. The decrease of Fo in olivine and La_{CN}/Sm_{CN} ratio associated to an increase of the CaO content in olivine and Gd_{CN}/Yb_{CN} ratio in pure dunites (Figs. 6 and 7) was previously attributed to the percolation of MORB and subsequent reequilibration with the surrounding olivine (Abily and Ceuleneer, 2013; Rospabé et al., 2018a). This implies the overprint of a MORB signature over a prior enriched signature potentially related to the genesis of small melt batches enriched in H_2O, silica and incompatible trace elements during the early dunitization (Rospabé et al., 2018a). This interpretation is also supported by the fractionation of U/Th and Nb/Ta ratios from the dunitic horizons toward fault zones (decrease of U/Th and increase of Nb/Ta toward faults with few exceptions; Fig. 7), considering that U is known to be a fluid/hydrous melt mobile element and Ta is likewise expected to be much more easily mobilized by hydrous fluids or melts than by dry (or slightly hydrated) melt - MORB in our case - relative to Nb (Green, 1995). Evolutions of the chemical composition of the dunitic matrix, as well as of impregnant minerals (chromite, clinopyroxene, orthopyroxene and amphibole) at the approach of fault zones indicates that syn-magmatic faults conditioned the nature of the melt that circulated through the DTZ. A reasonable way to account for these observations is to envision a hybridization process between different melt batches within fault zones, which hence leads to an evolving reequilibration signature within the host olivine matrix, i.e. starting from faults and propagating into the surrounding dunitic horizons.

The introduction of hydrous fluids into the DTZ from above at an early magmatic stage is strongly supported by the petrological sequences along both cross-sections #1 and #3: interstitial orthopyroxene and amphibole appear in the shallowest levels of the DTZ, just above fault zones (N130 in the case of cross-section #1, N155 in the case of cross-section #3). This observation was previously attributed to the hybridization of upwelling MORB with downwelling hydrothermal fluids and/or hydrated silica-rich melts issued from the hydrous melting of surrounding rocks, with an increase of the hydrothermal component upsection (Rospabé et al., 2017). The correlation between syn-magmatic faults (see paragraph 4.1) and the appearance of minerals indicative of a hydrated magmatic environment supports that the

DTZ was continuously hydrated all along its development thanks to fracturing, from the prior dunitization stage until the later stage when more and more percolating melts invaded the DTZ. Finally, along fault zones occurs the hybridization between (1) the first interstitial H_2O- and silica-rich melts batches, (2) MORB issued from the deeper mantle partial melting and drained along faults through the DTZ, and (3) possibly continuous supply of hydrothermal fluids. The low Nb/Ta ratios within pure dunitic horizons (Fig. 7) may reflect melt-rock reaction at low melt/rock ratio (see Kelemen et al. (1993) concerning arc magmas generation and evolution, and Rospabé et al. (2018) concerning the present Maqsad DTZ), and/or that the early hydrated, enriched melt has fractionated a small amount of hydrous and Ti-rich minerals such as amphibole or mica (Bodinier et al., 1996; Green, 1995) prior to the reequilibration with the surrounding dunitic matrix. This later hypothesis is in accordance with (1) the assumption that this exotic melt was involved in the transport and the widespread fractionation of chromite at Moho level, chromite that entrapped inclusions of amphibole and mica (Rospabé et al., 2017; 2018), and (2) the observation of an increasing amount of chromite, especially as schlierens, approaching the faults (Figs. 3 and 4B; see also the vertical evolution of Cr in whole rock in the Electronic Supplement 2). It is worth noting that pure dunites that present a quite high Nb/Ta ratio while being located few tens of meters far from fault zones, chiefly at the base of the cross-section #1 (Fig. 7), generally correspond to samples containing schlierens of chromite (see the correspondence between the whole rock Cr content and HFSE ratios in the Electronic Supplement 2) that contain Ti-rich mineral inclusions. At a much larger scale, chromitite deposits were regularly observed along major shear zones within the DTZ and the uppermost part of the mantle section of the Oman ophiolite (Boudier and Al-Rajhi, 2014; Zagrtdenov et al., 2018).

4.2.2. Faulting and refertilization

Accordingly, the fact that the cross-section #2, in intermediate location between sections #1 and #3 (Figs. 1B and 3), is more impregnated all the way up may be related to its peculiar structural situation. A large part of this section is enclosed in a graben structure, bordered by N130 fault zones with an opposite dip. Accordingly, we interpret this location as a main avenue for melt percolation, issued from the mantle partial melting, and for hydrothermal fluids circulation, introduced along fault zones. This led to strong fluid-melt-rock reactions and to the refertilization of the dunitic matrix, potentially linked to a temperature decrease within the graben structure. Contrariwise, pure dunitic horizons in sections 1 and 3 were compacted at higher temperature before massive crystallization from interstitial melts.

Clinopyroxene grains from samples collected few meters from faults preserve a chemical zoning while zoning is uncommon at larger distance (Fig. 8A). The occurrence or absence of zoning is unrelated to the modal composition of the rock and from the grain size and seems to depend only on the vicinity of a fault. Such chemical zonings in strongly impregnated peridotites (frequently described as "olivine-rich troctolites") collected along detachment faults in present-day ridges and in ophiolites were previously interpreted as the result of reactive crystallization (e.g. Drouin et al., 2009; Sanfilippo et al., 2015 and references therein), i.e. mineral fractionation associated to harzburgite orthopyroxene or dunite olivine assimilation (Collier and Kelemen, 2010). The importance of reactive crystallization relative to fractional crystallization was previously considered as limited in the case of the Maqsad DTZ (Rospabé et al., 2018a). Nonetheless, our results allow us to consider that, even if the refertilization process was dominated by fractional crystallization from percolating melts, the development of syn-magmatic fault zones during the DTZ formation reinforced local (fluid-)melt-rock reactions triggering reactive crystallization. Therefore, we propose that strong relationships between the structural environment and mantle refertilization may be the key to decipher the origin of hybrid olivine-rich troctolites along oceanic core complex (Sanfilippo et al., 2015 and references therein).

4.3. Implications for the development of the DTZ and melt migration beneath spreading centres

The progressive chemical evolution vertically along the DTZ, starting from a enriched melt and acquiring progressively a MORB signature, reflects that the hybridization between different melt batches is enhanced in fault zones that are avenues for both melt and fluids circulations. The syn-magmatic faults affecting the DTZ, whatever their orientation but with a dipping frequently higher than 60°, may have assisted the MORB extraction from the Maqsad diapir. In this way, the most salient MORB signature is markedly recorded in dunites located close to N165-N180 fault zones (e.g. higher CaO values; Fig. 6), the percolation having potentially been facilitated by the transtensional feature. Moreover, troctolite intrusions observed in the highest levels of the DTZ might represent the last extracted melt batches, which suffered fractional crystallization due to cooling. In other words, it appears that the DTZ recorded the switch between different melt extraction modes, starting with pervasive porous flow within the host dunite (strongest MORB-reequilibrated signature at the approach of faults), then followed in time when temperature decreases by melt discharges focused along fault zones (cumulate troctolite intrusions). In Figure 9 we propose a synthetic scenario for the DTZ formation above the Maqsad diapir:

- Stage A: Fault zones (important dipping, slight displacement) affect the DTZ early. They allow the introduction of fluids at Moho level that potentially assist the orthopyroxene melting out, leading to the mantle harzburgite transformation into dunite (Rospabé et al., 2017), and to the early generation of small volume of H_2O-, SiO_2 and incompatible trace elements enriched melts (Rospabé et al., 2018a).

- Stages B and C: Subsequently, fault zones focus the percolation of MORB issued from the continuous partial melting of mantle peridotites, allowing (1) to a more or less strong chemical reequilibration with host dunite, (2) to their hybridization with prior enriched melt which has a direct influence on the Cr redistribution at Moho level, (3) to their accumulation at certain levels, and (4) to the refertilization of the host dunite, mainly to the top of the DTZ, with anhydrous or hydrated minerals fractionation interstitially (fractional or reactive crystallization).

-Stage D: In addition to their strong influence on fluid-melt-rock reactions at Moho level, fault zones drain residual melts from the DTZ to the lower crust. Plurimetric intrusions of cumulate troctolites, becoming more and more abundant in the uppermost DTZ, are witnesses of these melt discharges before/during the magmatic activity cessation.

Beyond the structural control on the magmatic processes that occur within the oceanic Moho, fault zones continued to focus fluid circulation at lower temperature after the cessation of the magmatic activity. In addition to the Cr transport at high temperature and its massive fractionation as chromitite ore bodies that may have occurred preferentially along fault zones (Boudier and Al Rajhi, 2014; Zagrtdenov et al., 2018), later hydrothermal circulations along long-standing fractures should have led to strong chemical exchanges during low temperature alteration of the lower crust (Zihlmann et al., 2018) and serpentinization and carbonation at Moho level.

5. Conclusion

The fluid-melt-rocks reactions occurring at the mantle-crust transition below oceanic spreading centers are expected to significantly influence the nature of the melts that feed the crust and the chemical exchanges between the deep lithosphere and superficial envelopes. Our combined structural, petrological and geochemical study of the DTZ in the Sumail massif reveals that syn-magmatic tectonic lineaments primarily control these reactions. The Maqsad DTZ evolved in a transtensional environment induced by two N130 and N165-180 fault systems related to the complex (asymmetric) oceanic accretion geometry. Surprisingly, both systems seem to have influenced the petrological and geochemical organization of the DTZ, supporting their contemporaneity as formulated on the basis of field evidence. They both govern:

(1) the vertical chemical evolutions recorded in the olivine matrix and the interstitial minerals over tens of meters approaching faults zones, concerning elements considered immobile in fluids or during alteration such as REE, HFSE or Th (i.e. reflecting the overprint of several processes: the prior dunitization process, the focused migration of interstitial melts and/or fluids through the dunitic matrix along fault zones, and the modification of the percolating melt chemistry by hybridization);

(2) the petrological organization of the DTZ (i.e. the succession of pure and impregnated horizons, that reflects the spatial distribution of melt crystallization products).

In this frame, the fact that faults affect syn-magmatically the mantle-crust transition zone may be considered as the missing link between high temperature magmatic-related chemical imprints in DTZ dunites, the evident involvement of a hydrous component, the migration and extraction of percolating melts, and the mobilization and precipitation of a high amount of Cr within this interface. Moreover, the successive melt discharges from the DTZ to the crust, following different extraction modes, may have potentially contributed to the heterogeneity observed in the Oman ophiolite crust (Jansen et al., 2018) and along oceanic spreading centers worldwide.

Finally, syn-magmatic faults may have a great effect on the thermal and rheological structure of the oceanic lithosphere while they also apparently strongly influence chemical geodynamics (metals, sulfur and carbon cycles and so on) in oceanic ridges environment since fluids are introduced continuously along fault zones, from (more or less hydrated) magmatic stage to later, low temperature serpentinization and carbonation related to solely seawater-derived hydrothermal circulations. These findings may contribute to better understand the connection between the petrological, chemical and alteration reactions at Moho level and within the lower oceanic crust, and the thermal, tectonic and rheological structure of the whole oceanic lithosphere.

Acknowledgments

We would like to thank F. de Parseval, J.-F. Ména and L. Menjot for thin sections preparation and, for technical assistance during sample preparation and data acquisition, M. Henry and Jonathan Prunier (cleanroom lab), S. Gouy, J. Langlade and Ph. de Parseval (microprobe analysis), F. Candaudap (HR-ICP-MS for whole rock trace elements analysis) and D. Roggero (LA-ICP-MS for clinopyroxene trace elements analysis). We are grateful to H. Al Azri for its hospitality, as well as to M. Al Araimi, M. Al Batashi, A. Al-Rajhi, S. Almusharrafi and other colleagues from the Ministry of Commerce and Industry, Sultanate of Oman, for their kind support. We greatly thank A. Sanfilippo and an anonymous reviewer for their constructive comments, as well as T. A. Mather for editorial handling and comments, which helped to improve this manuscript. This work has benefited from a financial support provided by the Centre National de la Recherche Scientifique-Institut National des Sciences de l'Univers (CNRS-INSU).

Figure 1. (A) Simplified geological map of the Sumail massif (modified after Béchennec et al. (1992) and Wyns et al. (1992)). The massif exposes a N130-oriented paleo-ridge spreading centre. It is centred on a mantle paleo-diapir structure defined by the vertical mantle flow

structure observed in the Maqsad area (Ceuleneer et al., 1988; Jousselin et al., 1998). The dunitic transition zone is well exposed along the ridge axis and to the SW between the ridge axis and the N165 ductile Muqbariah fault system. The white rectangle highlights our study area. (B) Detailed geological map of the studied area (modified after Rabu et al. (1986)). The dunitic transition zone (DTZ) is more than 300 m thick along the ridge axis. The three studied cross-sections (cross-sections #1, #2 and #3 from north to south) were sampled from the wadi Mahram to the west to the higher levels of the DTZ to the east. The sampling density we adopted (step of 10 to 20 meters of elevation) has been previously shown to be optimal to the description of the vertical petrological and geochemical variability through the DTZ (Abily and Ceuleneer, 2013; Rospabé, 2018), particularly in the Sumail massif where the paleo-Moho is sub-horizontal with a weak ESE regional dip (i.e. current absolute altitudes correspond closely to paleo-depth). Structural measurements completed during our field exploration are also reported on this sketch, especially the dipping and the dipping direction along the two N130 and N165-N180 main fault systems identified in this area. The along strike extent of the main faults exceeds several kilometers.

Figure 2. Three examples of relationships between deformed magmatic features and N130 (A) or N165-180 (B and C) fault zones affecting the DTZ in the studied area. A) A layered troctolite lens is offset by about few meters along a N130.70NE normal fault making the contact with surrounding dunite (left). These mafic cumulates recorded a strong deformation near the fault plane (centre) while plagioclases show a remarkable elongation within the groundmass (right). B) Deformation of magmatic products in the tectonic corridor located at the base of the studied cross-sections and separating the DTZ from the harzburgite mantle section (Fig. 1B). Among others, we observed an elongated gabbroic boudin (top) or flames structures displayed by gabbros laminated within the host dunite (centre) along the N180.80W

fault, as well as aligned and elongated plagioclase impregnations in dunites (bottom) along the N165.85E major fault. C) A N165.80W fault zone cross-cutting the cross-section #1 is characterized by a well organized schistose parting in dunites (left) with no evidence of mylonitic deformation (right top). An undeformed amphibole-bearing gabbroic dike, oriented N125.70NE, cross-cut the schistosity of the N165.80W fault zone (right bottom).

Figure 3. Petrological and structural logs of the three studied cross-sections: from north to south the section #1 (293 m), the section #2 (343 m) and the section #3 (371 m). Regardless of the petrological sequences of the DTZ - a lower pure dunitic half surmounted by an impregnated half (cross-sections #1 and #3), or more extensively impregnated (cross-section #2) -, the transition from a lithological facies to another generally corresponds to the presence of a fault zone. There is no systematics between the direction of the fault, N130 or N165-180, and the minerals distribution.

Figure 4. Photomicrographs showing the different mineral contents characterizing the DTZ dunites in the Maqsad area, with A) a "pure dunite", almost made of olivine and chromite only and containing a very few amount (<0.5%) of small (few hundreds microns at most) clinopyroxene rims between two olivine grains or located at 120° olivine grains triple junctions (16OM07A - cross-section #3), B) a dunite containing chromite organized as schlierens (16OM24A - cross-section #3), C) an orthopyroxene oikocryst in an opx/pl/cpx-bearing dunite (16OM29 - cross-section #3), D) a part of a clinopyroxene oikocryst up to 5 mm in a strongly impregnated pl/cpx-bearing dunite (16OM49 - cross-section #2), and E) interstitial amphibole in an amph-bearing dunite (± opx/pl/cpx) (16OM74B - cross-section #2).

Figure 5. Chemical variations along cross-sections 1, 2 and 3 in the Maqsad dunitic transition zone (data for cross-section 1 are from Rospabé et al. (2018), data for cross-sections 2 and 3 are newly presented here). A) NiO content as a function of Fo in olivine, B) whole rock chondrite-normalized REE and Primitive Mantle-normalized multi-elements patterns of pure dunites (in the middle) and impregnated dunites (at the bottom). The precision is better than 10% for LILE, REE, Pb, Th and U, and better than 20% for HFSE (see also Rospabé et al., 2018b). Grey fields represent the entire variation ranges described in Rospabé et al. (2018). Analytical methods used to acquire the data are detailed in the Electronic Supplement 1. Chondrite and Primitive Mantle normalizing values are from Barrat et al. (2012) and Sun and McDonough (1989) respectively.

Figure 6. Vertical evolution of the mineral chemical composition along the studied cross-sections, plotted as a function of the altitude. The colours of the dots represent the different lithological facies, with pure dunites in blue, cpx-bearing dunites in red, pl/cpx-bearing in orange, opx/pl/cpx-bearing dunite in purple and amph-bearing dunites in green. Red dashed lines are faults, each being localized where they respectively cut across each section. The grey gradient highlights the vertical increasing or decreasing characteristic of each element or element ratio, in some case related to the presence of fault zones. Are represented the Fo (100 × molar $Mg/(Mg + Fe_{total})$) and the CaO content (wt.%) in olivine, the XCr (100 × molar Cr/(Cr + Al)) in chromite and the TiO_2 content (wt.%) in clinopyroxene. Mineral compositions for samples from the cross-section #1 are issued from Rospabé et al. (2018), corresponding to the "Buri cross-section". The amount of impregnation is also reported to the left as a function of the altitude. The modal content, available in Supplementary Table 1, was calculated using the MINSQ least squares method (Herrmann and Berry, 2002) based on whole rock and minerals major element compositions.

Figure 7. Vertical evolution of the whole rock chemical composition along the studied cross-sections, plotted as a function of the altitude. The colours of the dots represent the different lithological facies, with pure dunites in blue, cpx-bearing dunites in red, pl/cpx-bearing in orange, opx/pl/cpx-bearing dunite in purple and amph-bearing dunites in green. Red dashed lines are faults, each being localized where they respectively cut across each section. The grey gradient highlights the vertical increasing or decreasing characteristic of each element or element ratio, in some case related to the presence of fault zones. Are represented the Mg# (100 × molar Mg/(Mg + Fe_{total})), La_{CN}/Sm_{CN}, Nb/Ta and U/Th ratios. Chondrite normalizing values used to calculate the La_{CN}/Sm_{CN} ratio are from Barrat et al. (2012). Whole rock compositions for samples from the cross-section #1 are issued from Rospabé et al. (2018), corresponding to the "Buri cross-section". The amount of impregnation is also reported to the left as a function of the altitude. The modal content, available in Supplementary Table 1, was calculated using the MINSQ least squares method (Herrmann and Berry, 2002) based on whole rock and minerals major element compositions.

Figure 8. Magnesium number (Mg# = 100 × molar Mg/(Mg + Fe^{2+})) and SiO_2, Al_2O_3, Cr_2O_3 and TiO_2 concentration profile across two clinopyroxenes from opx/pl/cpx-bearing dunites (15OM03A to the left, 16OM26 to the right). A) The first one to the left shows a well-defined composition zoning with an increase of Mg# and SiO_2 and TiO_2 contents, together with the decrease of Al_2O_3 and Cr_2O_3, from core to rims. This pattern is similar to what is observed in the case of reactive crystallization in abyssal olivine-rich troctolites, when the surrounding peridotite is partly assimilated during fractional crystallization (Sanfilippo et al., 2015 and reference therein). B) The second one to the right exhibits patterns more random in Mg#, flattest in SiO_2 and TiO_2, and similar to the first one in Al_2O_3 and Cr_2O_3 with the same

decrease toward grain rims.

Figure 9. Synthetic model for the DTZ vertical structuration in the Maqsad area. Stage A: Introduction of fluids at Moho level along fault zones which potentially assist the upper mantle dunitization (Rospabé et al., 2017) and, consequently, leads to the generation of small melts batches enriched in H_2O-, SiO_2 and incompatible trace elements (Rospabé et al., 2018a). Stage B: Ascending MORB percolation focused along fault zones, hybridization between MORB and the early interstitial enriched melt, reequilibration with the surrounding dunitic matrix, melt accumulation and interstitial mineral crystallization in the upper levels of the DTZ (fractional or reactive crystallization depending on the distance to faults). Stage C: Fractionation of hydrous minerals, or anhydrous minerals witnessing of hydrous melts percolation, following the continuous hybridization between MORB and other exotic melts through the DTZ. This hybrid melt is involved in the mobilization and precipitation of Cr. Note that stages B and C may be contemporaneous since it has been evidenced that exotic H_2O- and SiO_2-rich melt were involved as early as the dunitization itself (Rospabé et al., 2017; 2018). The two stages were here decoupled to make easier the understanding of the structural, petrological and geochemical organization of the DTZ. Stage D: Residual melts extraction from the DTZ to the crust, with the formation of entrapment zones represented by cumulate troctolite intrusions at the top of the DTZ. Subsequent alteration (serpentinization, carbonation) of the DTZ dunites, especially along faults and fractures, follows the magmatic activity cessation.

References

Abily, B., Ceuleneer, G., 2013. The dunitic mantle-crust transition zone in the Oman ophiolite: Residue of melt-rock interaction, cumulates from high-MgO melts, or both?

Geology 41, 67-70. doi:10.1130/G33351.1

Abily, B., Ceuleneer, G., Launeau, P., 2011. Synmagmatic normal faulting in the lower oceanic crust: Evidence from the Oman ophiolite. Geology 39, 391-394. doi:10.1130/G31652.1

Akizawa, N., Arai, S., Tamura, A., Uesugi, J., Python, M., 2011. Crustal diopsidites from the northern Oman ophiolite: Evidence for hydrothermal circulation through suboceanic Moho. J. Mineral. Petrol. Sci. 106, 261-266. doi:10.2465/jmps.110621b

Amri, I., 1995. Etude pétrologique et structurale d'une dorsale océanique fossile, Massif de Sumail (ophiolite d'Oman). Implications pour les mécanismes d'accrétion océanique. Université Paul Sabatier, Toulouse III.

Amri, I., Benoit, M., Ceuleneer, G., 1996. Tectonic setting for the genesis of oceanic plagiogranites: evidence from a paleo-spreading structure in the Oman ophiolite. Earth Planet. Sci. Lett. 139, 177-194. doi:10.1016/0012-821X(95)00233-3

Barrat, J.-A., Zanda, B., Moynier, F., Bollinger, C., Liorzou, C., Bayon, G., 2012. Geochemistry of CI chondrites: Major and trace elements, and Cu and Zn Isotopes. Geochim. Cosmochim. Acta 83, 79-92. doi:10.1016/j.gca.2011.12.011

Béchennec, F., Roger, J., Le Métour, J., Wyns, R., 1992. Geological Map of Seeb: Sheet NF 40-03, Scale: 1:250,000. Explanatory Notes. Dir. Gen. Miner. Oman Minist. Pet. Miner.

Benoit, M., Ceuleneer, G., Polvé, M., 1999. The remelting of hydrothermally altered peridotite at mid-ocean ridges by intruding mantle diapirs. Nature 402, 514-518. doi:10.1038/990073

Benoit, M., Polvé, M., Ceuleneer, G., 1996. Trace element and isotopic characterization of mafic cumulates in a fossil mantle diapir (Oman ophiolite). Chem. Geol. 134, 199-214. doi:10.1016/S0009-2541(96)00087-3

Bodinier, J.L., Merlet, C., Bedini, R.M., Simien, F., Remaidi, M., Garrido, C.J., 1996.

Distribution of niobium, tantalum, and other highly incompatible trace elements in the lithospheric mantle: The spinel paradox. Geochim. Cosmochim. Acta 60, 545-550. doi:10.1016/0016-7037(95)00431-9

Bosch, D., Jamais, M., Boudier, F., Nicolas, A., Dautria, J.M., Agrinier, P., 2004. Deep and high-temperature hydrothermal circulation in the Oman ophiolite-petrological and isotopic evidence. J. Petrol. 45, 1181-1208. doi:10.1093/petrology/egh010

Boudier, F., Al-Rajhi, A., 2014. Structural control on chromitite deposits in ophiolites: the Oman case. Geol. Soc. London, Spec. Publ. 392, 263-277. doi:10.1144/SP392.14

Boudier, F., Ceuleneer, G., Nicolas, A., 1988. Shear zones, thrusts and related magmatism in the Oman ophiolite: Initiation of thrusting on an oceanic ridge. Tectonophysics 151, 275-296. doi:10.1016/0040-1951(88)90249-1

Boudier, F., Nicolas, A., 1995. Nature of the moho transition zone in the Oman ophiolite. J. Petrol. 36, 777-796. doi:10.1093/petrology/36.3.777

Ceuleneer, G., 1991. Evidence for a Paleo-Spreading Center in the Oman Ophiolite: Mantle Structures in the Maqsad Area. Springer Netherlands, pp. 147-173. doi:10.1007/978-94-011-3358-6_9

Ceuleneer, G., Le Sueur, E., 2008. The Trinity ophiolite (California): the strange association of fertile mantle peridotite with ultra-depleted crustal cumulates. Bull. Soc. Géol. Fr. 179, 503-518. doi:10.2113/gssgfbull.179.5.503

Ceuleneer, G., Monnereau, M., Amri, I., 1996. Thermal structure of a fossil mantle diapir inferred from the distribution of mafic cumulates. Nature 379, 149-153. doi:10.1038/379149a0

Ceuleneer, G., Nicolas, A., 1985. Structures in podiform chromite from the Maqsad district (Sumail ophiolite, Oman). Miner. Depos. 20, 177-184. doi:10.1007/BF00204562

Ceuleneer, G., Nicolas, A., Boudier, F., 1988. Mantle flow pattern at an oceanic spreading centre: the Oman peridotite record. Tectonophysics 151, 1-26. doi:10.1016/0040-1951(88)90238-7

Clénet, H., Ceuleneer, G., Pinet, P., Abily, B., Daydou, Y., Harris, E., Amri, I., Dantas, C., 2010. Thick sections of layered ultramafic cumulates in the Oman ophiolite revealed by an airborne hyperspectral survey: Petrogenesis and relationship to mantle diapirism. Lithos 114, 265-281. doi:10.1016/j.lithos.2009.09.002

Collier, M. L., Kelemen, P. B., 2010. The case for reactive crystallization at mid-ocean ridges. J. Petrol. 51, 1913-1940. doi:10.1093/petrology/egq043

Currin, A., Wolff, P. E., Koepke, J., Almeev, R. R., Zhang, C., Zihlmann, B., Ildefonse, B., Teagle, D. A., 2018. Chlorine-rich amphibole in deep layered gabbros as evidence for brine/rock interaction in the lower oceanic crust: A case study from the Wadi Wariyah, Samail Ophiolite, Sultanate of Oman. Lithos 323, 125-136. doi:10.1016/j.lithos.2018.09.015

Drouin, M., Godard, M., Ildefonse, B., Bruguier, O., Garrido, C.J., 2009. Geochemical and petrographic evidence for magmatic impregnation in the oceanic lithosphere at Atlantis Massif, Mid-Atlantic Ridge (IODP Hole U1309D, 30°N). Chem. Geol. 264, 71-88. doi:10.1016/j.chemgeo.2009.02.013

France L., Ildefonse B., Koepke J., 2013. Hydrous magmatism triggered by assimilation of hydrothermally altered rocks in fossil oceanic crust (northern Oman ophiolite). Geochem. Geophys. Geosyst., 14, 2598-2614. doi:10.1002/ggge.20137

France L., Ildefonse B., Koepke J., 2009. Interactions between magma and hydrothermal system in Oman ophiolite and in IODP Hole 1256D: fossilization of a dynamic melt lens at fast spreading ridges. Geochem. Geophys. Geosyst., 10, Q10019. doi: 10.1029/2009GC002652

Gente, P., Pockalny, R. A., Durand, C., Deplus, C., Maia, M., Ceuleneer, G., Mével, C, Cannat, M, Laverne, C., 1995. Characteristics and evolution of the segmentation of the Mid-Atlantic Ridge between 20°N and 24°N during the last 10 million years. Earth Planet. Sci. Lett. 129, 55-71. doi:10.1016/0012-821X(94)00233-O

German, C.R., Petersen, S., Hannington, M.D., 2016. Hydrothermal exploration of mid-ocean ridges: Where might the largest sulfide deposits be forming? Chem. Geol. 420, 114-126. doi:10.1016/j.chemgeo.2015.11.006

Gilgen S.A., Diamond L.W., Mercolli I., 2016. Sub-seafloor alteration: Timing, depth and stratigraphic distribution in the Semail ophiolite, Oman. Lithos, 260, 191-210. doi: 10.1016/j.lithos.2016.05.014

Glennie, K.W., Boeuf, M.G.A., Hughes Clarke, M.W., Moody-Stuart, M., Pilaar, W.F.H., Reinhardt, B.M., 1974. Geology of the Oman Mountains. Verh. van het K. Ned. Geol. Mijnbouwkd. Genoot. 31, 423 pp.

Green, T.H., 1995. Significance of Nb/Ta as an indicator of geochemical processes in the crust-mantle system. Chem. Geol. 120, 347-359. doi:10.1016/0009-2541(94)00145-X

Gregory, R.T., Taylor, H.P., 1981. An oxygen isotope profile in a section of Cretaceous oceanic crust, Samail Ophiolite, Oman: Evidence for δ18O buffering of the oceans by deep (>5 km) seawater-hydrothermal circulation at mid-ocean ridges. J. Geophys. Res. Solid Earth 86, 2737-2755. doi:10.1029/JB086iB04p02737

Herrmann, W., Berry, R. F., 2002. MINSQ - a least squares spreadsheet method for calculating mineral proportions from whole rock major element analyses. Geochemistry Explor. Environ. Anal. 2, 361-368. doi:10.1144/1467-787302-010

Jansen, M. N., Lissenberg, C. J., Klaver, M., de Graaff, S. J., Koornneef, J. M., Smeets, R. J., MacLeod, C.J., Davies, G. R. 2018. Isotopic variation in Semail Ophiolite lower crust reveals crustal-level melt aggregation. Geochem. Persp. Let. 8, 37-42. doi:10.7185/geochemlet.1827

Jousselin, D., Nicolas, A., Boudier, F., 1998. Detailed mapping of a mantle diapir below a paleo-spreading center in the Oman ophiolite. J. Geophys. Res. Solid Earth 103, 18153-18170. doi:10.1029/98JB01493

Kelemen, P.B., Shimizu, N., Dunn, T., 1993. Relative depletion of niobium in some arc magmas and the continental crust: partitioning of K, Nb, La and Ce during melt/rock reaction in the upper mantle. Earth Planet. Sci. Lett. 120, 111-134. doi:10.1016/0012-821X(93)90234-Z

Koepke, J., Feig, S. T., Snow, J, 2005. Hydrous partial melting within the lower oceanic crust. Terra Nova 17, 286-291. doi:10.1111/j.1365-3121.2005.00613.x

Koga, K.T., Kelemen, P.B., Shimizu, N., 2001. Petrogenesis of the crust-mantle transition zone and the origin of lower crustal wehrlite in the Oman ophiolite. Geochemistry, Geophys. Geosystems 2. doi:10.1029/2000GC000132

MacLeod, C.J., Rothery, D.A., 1992. Ridge axial segmentation in the Oman ophiolite: Evidence from along-strike variations in the sheeted dyke complex. Ophiolites Their Mod. Ocean. Analog. 60, 39-63. doi:10.1144/GSL.SP.1992.060.01.03

Nehlig, P., Juteau, T., 1988. Deep crustal seawater penetration and circulation at ocean ridges: Evidence from the Oman ophiolite. Mar. Geol. 84, 209-228. doi:10.1016/0025-3227(88)90102-8

Nicolas, A., Ceuleneer, G., Boudier, F., Misseri, M., 1988. Structural mapping in the Oman ophiolites: Mantle diapirism along an oceanic ridge. Tectonophysics 151, 27-56. doi:10.1016/0040-1951(88)90239-9

Pallister, J.S., 1981. Structure of the sheeted dike complex of the Samail Ophiolite near Ibra, Oman. J. Geophys. Res. Solid Earth 86, 2661-2672. doi:10.1029/JB086iB04p02661

Python, M., Ceuleneer, G., 2003. Nature and distribution of dykes and related melt migration structures in the mantle section of the Oman ophiolite. Geochemistry, Geophys.

Geosystems 4. doi:10.1029/2002GC000354

Python, M., Ceuleneer, G., Ishida, Y., Barrat, J.-A., Arai, S., 2007. Oman diopsidites: a new lithology diagnostic of very high temperature hydrothermal circulation in mantle peridotite below oceanic spreading centres. Earth Planet. Sci. Lett. 255, 289-305. doi:10.1016/j.epsl.2006.12.030

Quick, J. E., 1981. The origin and significance of large, tabular dunite bodies in the Trinity peridotite, northern California. Contrib. Mineral. Petrol. 78, 413-422. doi:10.1007/BF00375203

Rabu, D., Béchennec, F., Beurrier, M., Hutin, M., 1986. Geological Map of Nakhl: Sheet NF 40-3E, Scale: 1:100,000. Explanatory Notes. Dir. Gen. Miner. Oman Minist. Pet. Miner.

Reuber, I., 1988. Complexity of the crustal sequence in the northern Oman ophiolite (Fizh and southern Aswad blocks): The effect of early slicing? Tectonophysics 151, 137-165. doi:10.1016/0040-1951(88)90244-2

Rioux, M., Bowring, S., Kelemen, P., Gordon, S., Miller, R., Dudás, F., 2013. Tectonic development of the Samail ophiolite: High-precision U-Pb zircon geochronology and Sm-Nd isotopic constraints on crustal growth and emplacement. J. Geophys. Res. Solid Earth 118, 2085-2101. doi:10.1002/jgrb.50139

Rospabé, M., 2018. Etude pétrologique, géochimique et structurale de la zone de transition dunitique dans l’ophiolite d’Oman : Identification des processus pétrogénétiques à l’interface manteau/croûte. Université Paul Sabatier, Toulouse III.

Rospabé, M., Benoit, M., Ceuleneer, G., Hodel, F., & Kaczmarek, M. A., 2018a. Extreme geochemical variability through the dunitic transition zone of the Oman ophiolite: Implications for melt/fluid-rock reactions at Moho level beneath oceanic spreading centers. Geochim. Cosmochim. Acta 234, 1-23. doi:10.1016/j.gca.2018.05.012

Rospabé, M., Benoit, M., Candaudap, F., 2018b. Determination of Trace Element Mass

Fractions in Ultramafic Rocks by HR-ICP-MS: A Combined Approach Using a Direct Digestion/Dilution Method and Preconcentration by Coprecipitation. Geostand. Geoanalytical Res. 42, 115–129. doi:10.1111/ggr.12181

Rospabé, M., Ceuleneer, G., Benoit, M., Abily, B., Pinet, P., 2017. Origin of the dunitic mantle-crust transition zone in the Oman ophiolite: The interplay between percolating magmas and high-temperature hydrous fluids. Geology 45, 471-474. doi:10.1130/G38778.1

Sanfilippo, A., Tribuzio, R., Ottolini, L., Hamada, M., 2017. Water, lithium and trace element compositions of olivine from Lanzo South replacive mantle dunites (Western Alps): New constraints into melt migration processes at cold thermal regimes. Geochim. Cosmochim. Acta 214, 51-72. doi:10.1016/j.gca.2017.07.034

Sanfilippo, A., Morishita, T., Kumagai, H., Nakamura, K., Okino, K., Hara, K., Tamura, A., Arai, S., 2015. Hybrid troctolites from mid-ocean ridges: Inherited mantle in the lower crust. Lithos 232, 124-130. doi:10.1016/j.lithos.2015.06.025

Sanfilippo, A., Tribuzio, R., Tiepolo, M., 2014. Mantle-crust interactions in the oceanic lithosphere: Constraints from minor and trace elements in olivine. Geochim. Cosmochim. Acta 141, 423-439. doi:10.1016/j.gca.2014.06.012

Sinton, J., Bergmanis, E., Rubin, K., Batiza, R., Gregg, T.K.P., Gronvold, K., Macdonald, K.C., White, S.M., 2002. Volcanic eruptions on mid-ocean ridges: New evidence from the superfast spreading East Pacific Rise, 17 degrees-19 degrees S. J. Geophys. Res. Solid Earth 107. doi:10.1029/2000JB000090

Sun S.-S. and McDonough W. F., 1989. Chemical and isotopic systematics of oceanic basalts: implications for mantle composition and processes. Geol. Soc. Lond., Spec. Publ. 42, 313-345. doi:10.1144/GSL.SP.1989.042.01.19

Wyns, R., Béchennec, F., Chevrel, S., Le Métour, J., Roger, J., 1992. Geological Map of

Nazwa: Sheet NF 40-07, Scale: 1:250,000. Explanatory Notes. Dir. Gen. Miner. Oman Minist. Pet. Miner.

Yeo, I.A., Devey, C.W., LeBas, T.P., Augustin, N., Steinführer, A., 2016. Segment-scale volcanic episodicity: Evidence from the North Kolbeinsey Ridge, Atlantic. Earth Planet. Sci. Lett. 439, 81-87. doi:10.1016/j.epsl.2016.01.029

Zagrtdenov, N. R., Ceuleneer, G., Rospabé, M., Borisova, A. Y., Toplis, M. J., Benoit, M., & Abily, B., 2018. Anatomy of a chromitite dyke in the mantle/crust transition zone of the Oman ophiolite. Lithos, 312, 343-357. doi:10.1016/j.lithos.2018.05.012

Zhang, C., Koepke, J., France, L., Godard, M., 2017. Felsic Plutonic Rocks from IODP Hole 1256D, Eastern Pacific: Implications for the Nature of the Axial Melt Lens at Fast-Spreading Mid-Ocean Ridges. J. Petrol. 58, 1535-1565. doi:10.1093/petrology/egx064

Zihlmann, B., Müller, S., Coggon, R.M., Koepke, J., Garbe-Schönberg, D., Teagle, D.A., 2018. Hydrothermal fault zones in the lower oceanic crust: An example from Wadi Gideah, Samail ophiolite, Oman. Lithos 323, 103-124. doi:10.1016/j.lithos.2018.09.008

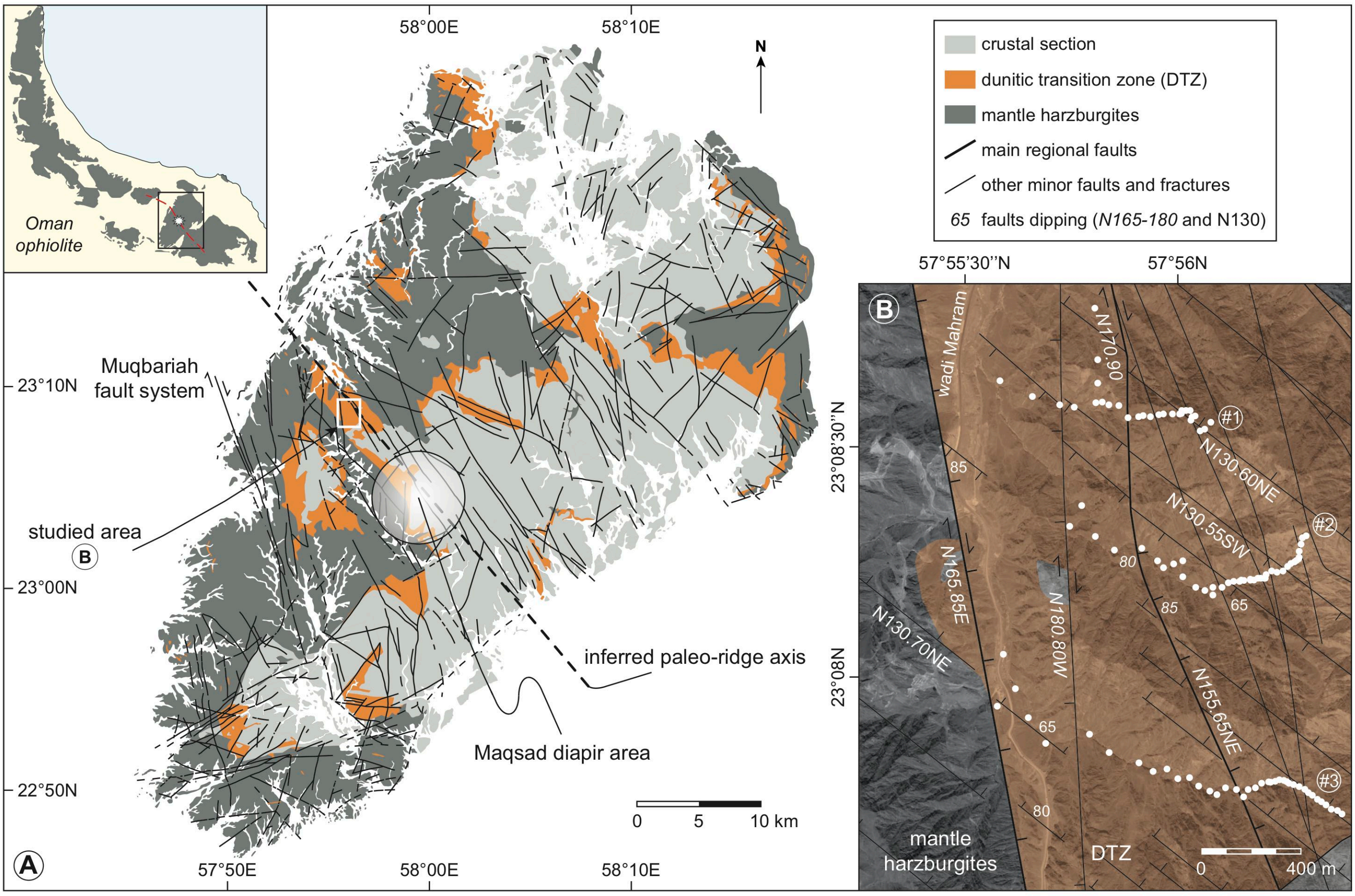

crustal section
dunitic transition zone (DTZ)
mantle harzburgites
main regional faults
other minor faults and fractures
65 faults dipping (N165-180 and N130)
Oman ophiolite
58°00E
58°10E
N
23°10N
23°00N
22°50N
57°50E
Muqbariah fault system
studied area
B
inferred paleo-ridge axis
Maqsad diapir area
0 5 10 km
A
57°55'30''N
57°56N
23°08'30"N
23°08N
Wadi Mahram
N170.90
#1
N130.60NE
#2
N130.55SW
N165.85E
N180.80W
N130.70NE
N155.65NE
#3
mantle harzburgites
DTZ
0 400 m

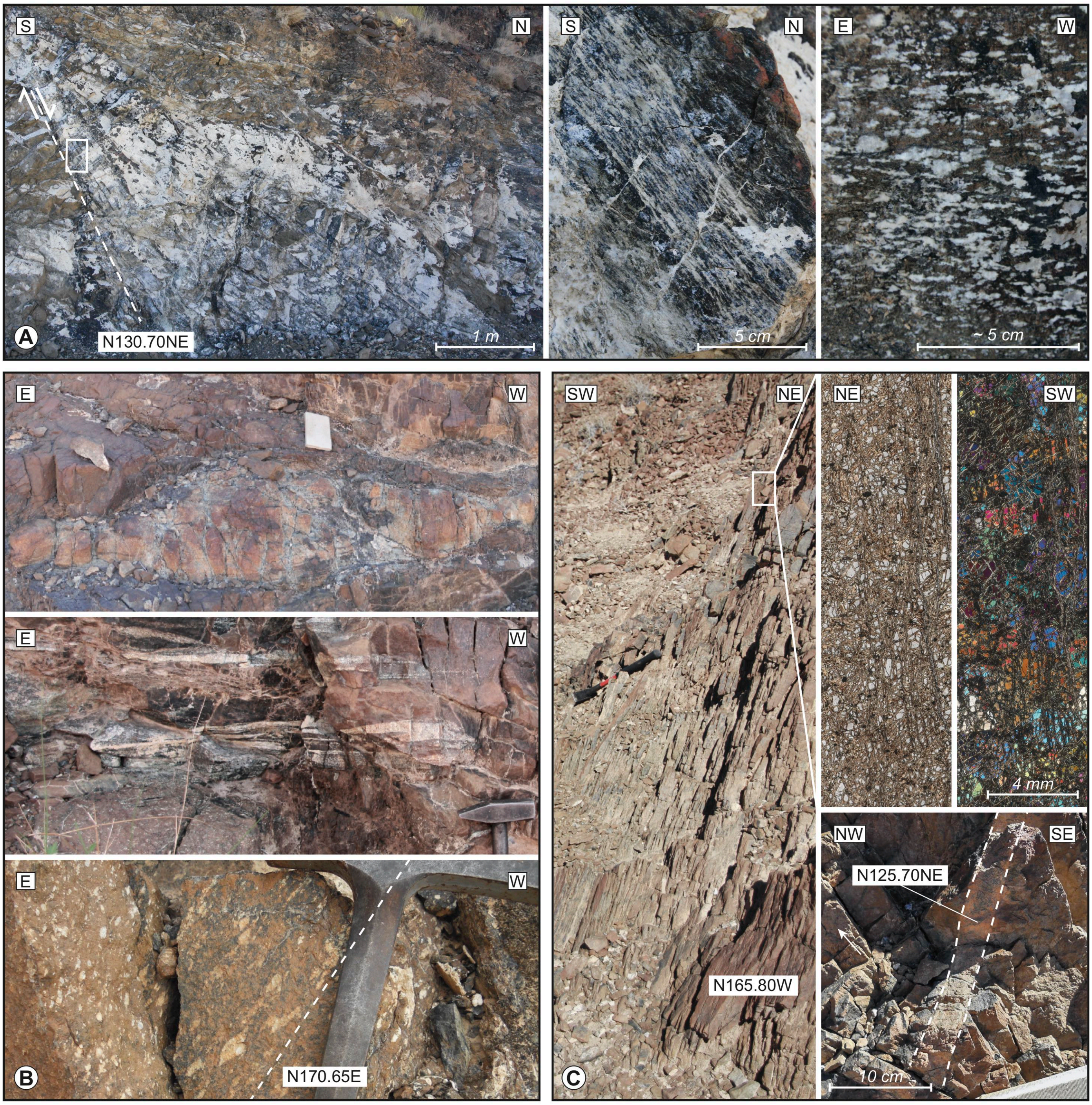
S
N
N130.70NE
1 m
A
S
N
5 cm
E
W
~ 5 cm
E
W
E
W
E
W
N170.65E
B
SW
NE
N165.80W
C
NE
SW
4 mm
NW
SE
N125.70NE
10 cm

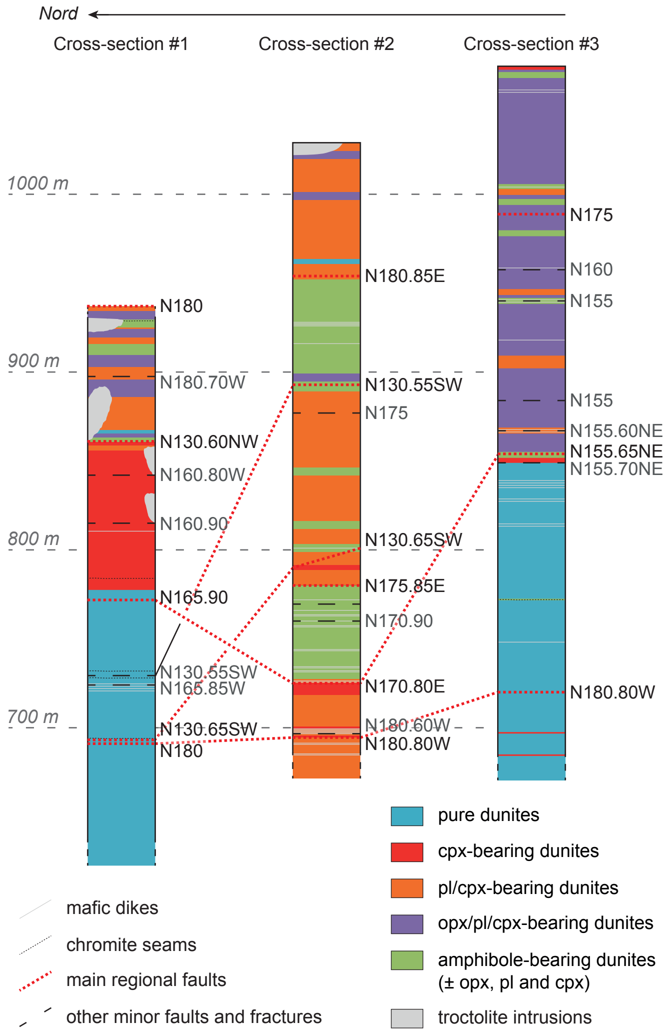

Nord
Cross-section #1
Cross-section #2
Cross-section #3
1000 m
900 m
800 m
700 m
N180
N180.70W
N130.60NW
N160.80W
N160.90
N165.90
N130.55SW
N165.85W
N130.65SW
N180
N180.85E
N130.55SW
N175
N130.65SW
N175.85E
N170.90
N170.80E
N180.60W
N180.80W
N175
N160
N155
N155
N155.60NE
N155.65NE
N155.70NE
N180.80W
pure dunites
cpx-bearing dunites
pl/cpx-bearing dunites
opx/pl/cpx-bearing dunites
amphibole-bearing dunites (± opx, pl and cpx)
troctolite intrusions
mafic dikes
chromite seams
main regional faults
other minor faults and fractures

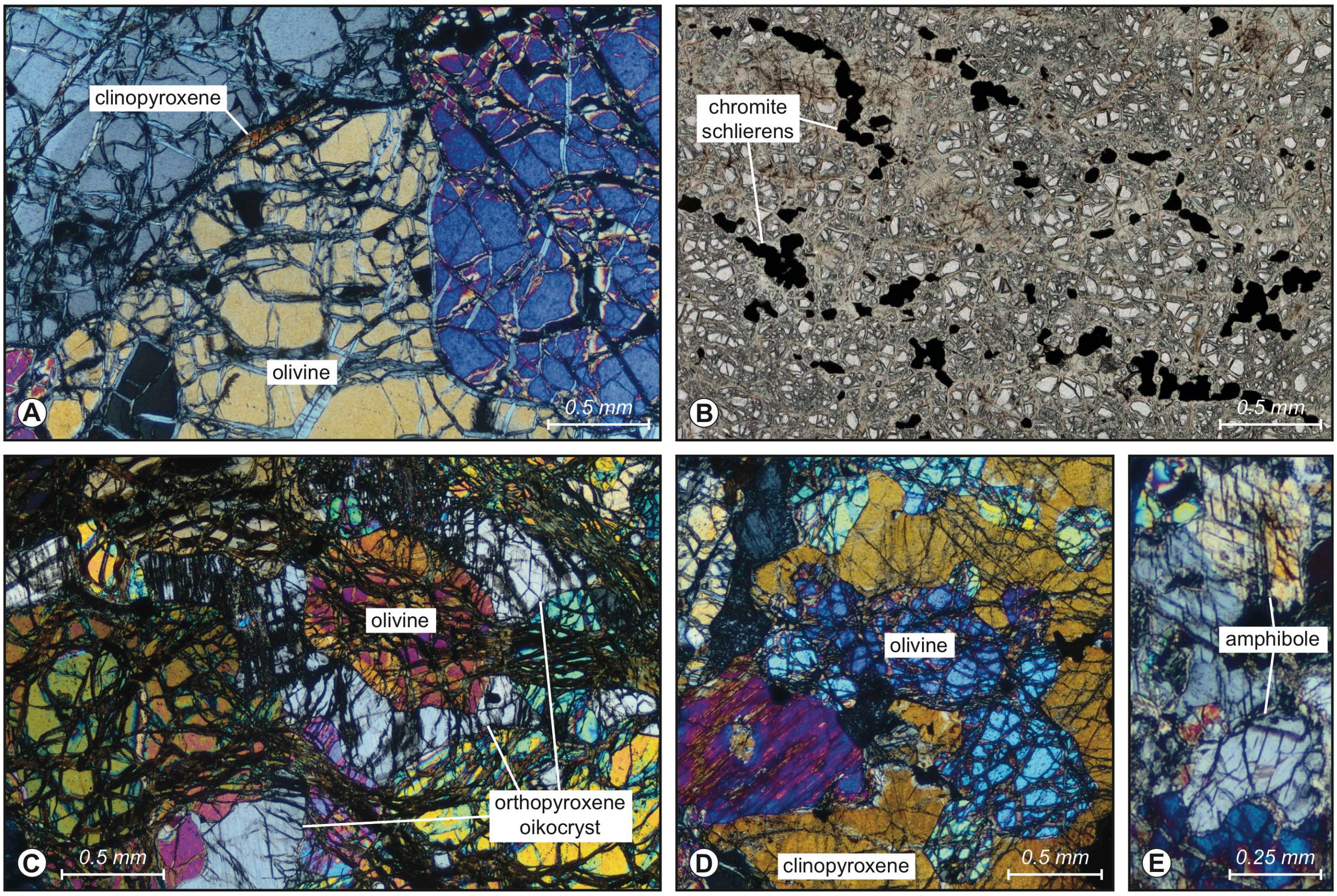
clinopyroxene
olivine
A
0.5 mm
chromite
schlierens
B
0.5 mm
olivine
orthopyroxene
oikocryst
C
0.5 mm
olivine
clinopyroxene
D
0.5 mm
amphibole
E
0.25 mm

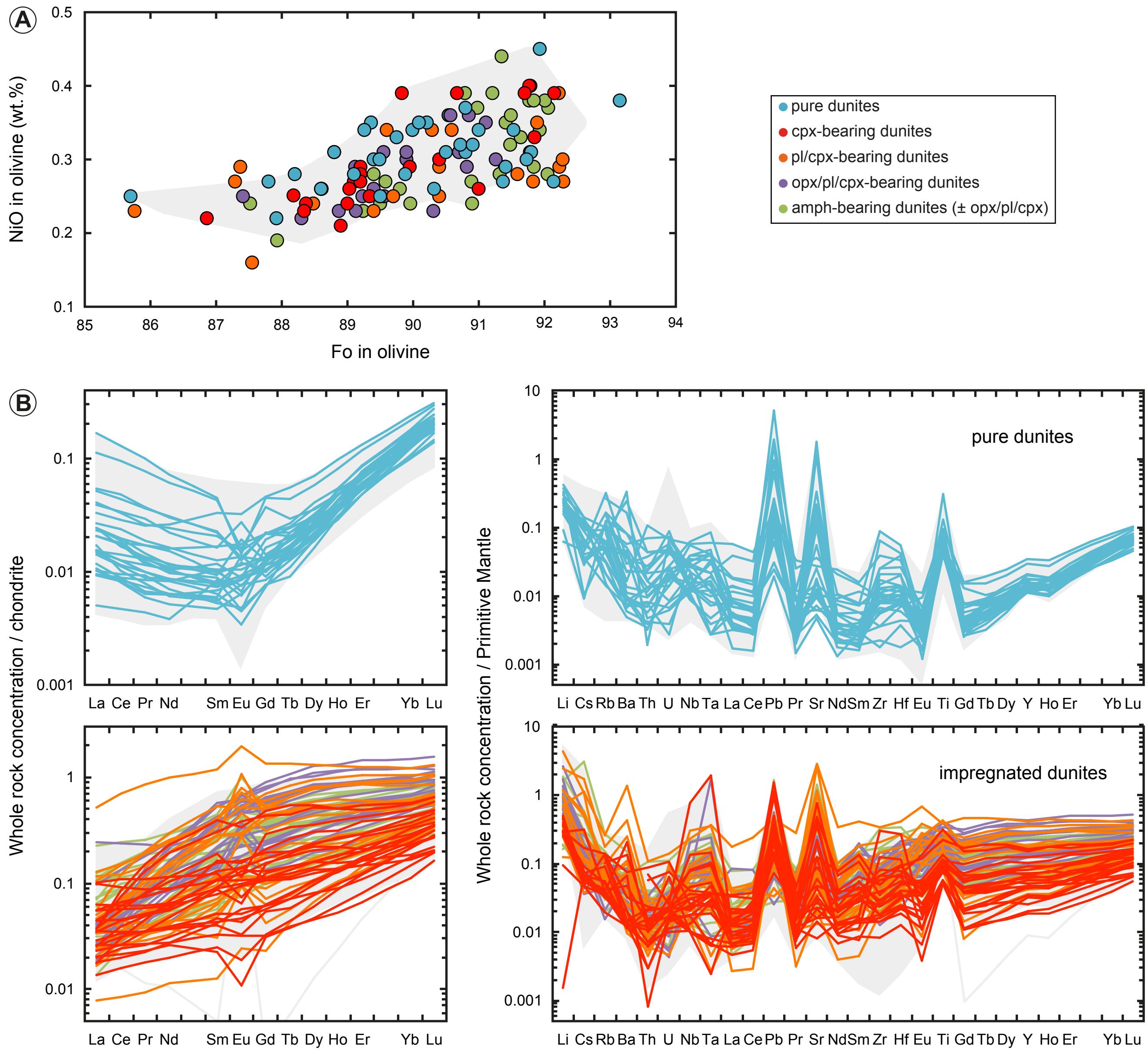
A
NiO in olivine (wt.%)
Fo in olivine
pure dunites
cpx-bearing dunites
pl/cpx-bearing dunites
opx/pl/cpx-bearing dunites
amph-bearing dunites (± opx/pl/cpx)
B
Whole rock concentration / chondrite
Whole rock concentration / Primitive Mantle
pure dunites
impregnated dunites
La Ce Pr Nd Sm Eu Gd Tb Dy Ho Er Yb Lu
Li Cs Rb Ba Th U Nb Ta La Ce Pb Pr Sr Nd Sm Zr Hf Eu Ti Gd Tb Dy Y Ho Er Yb Lu

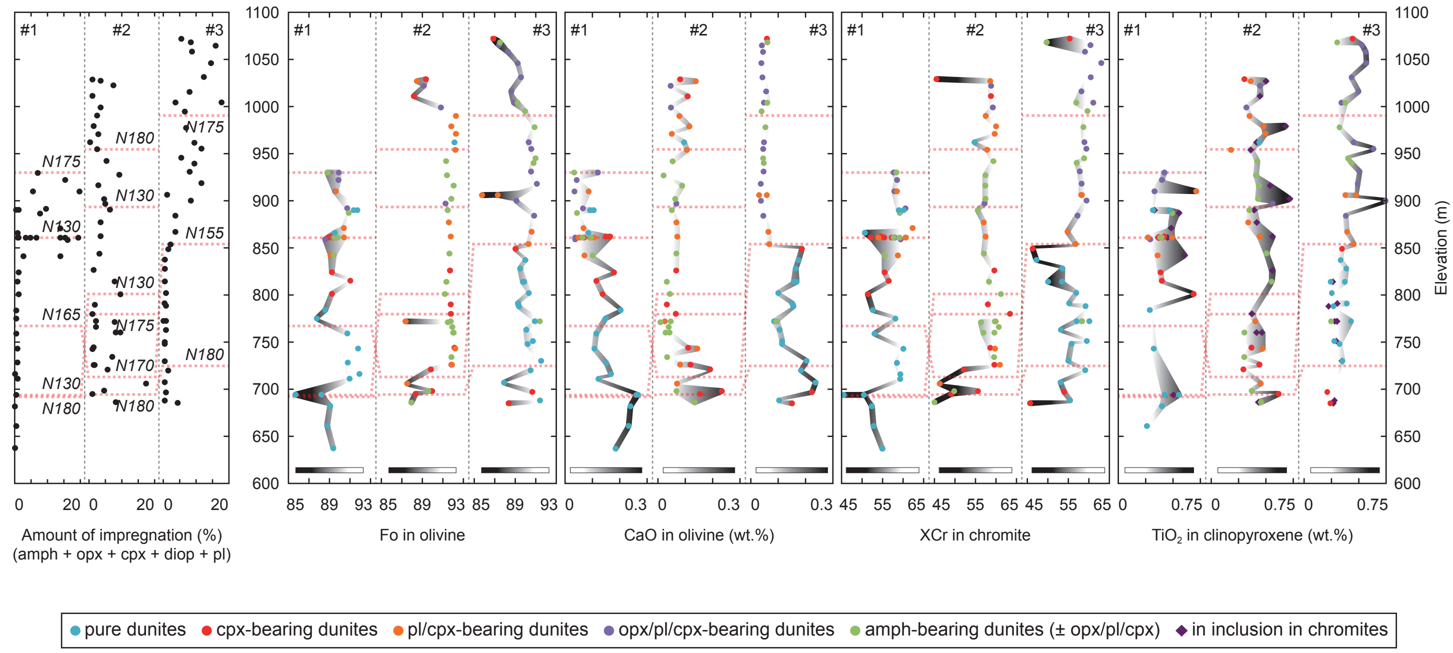
#1
#2
#3
N175
N180
N130
N130
N155
N130
N165
N175
N180
N170
N130
N180
N180
Amount of impregnation (%)
(amph + opx + cpx + diop + pl)
Fo in olivine
CaO in olivine (wt.%)
XCr in chromite
TiO2 in clinopyroxene (wt.%)
Elevation (m)
pure dunites
cpx-bearing dunites
pl/cpx-bearing dunites
opx/pl/cpx-bearing dunites
amph-bearing dunites (± opx/pl/cpx)
in inclusion in chromites

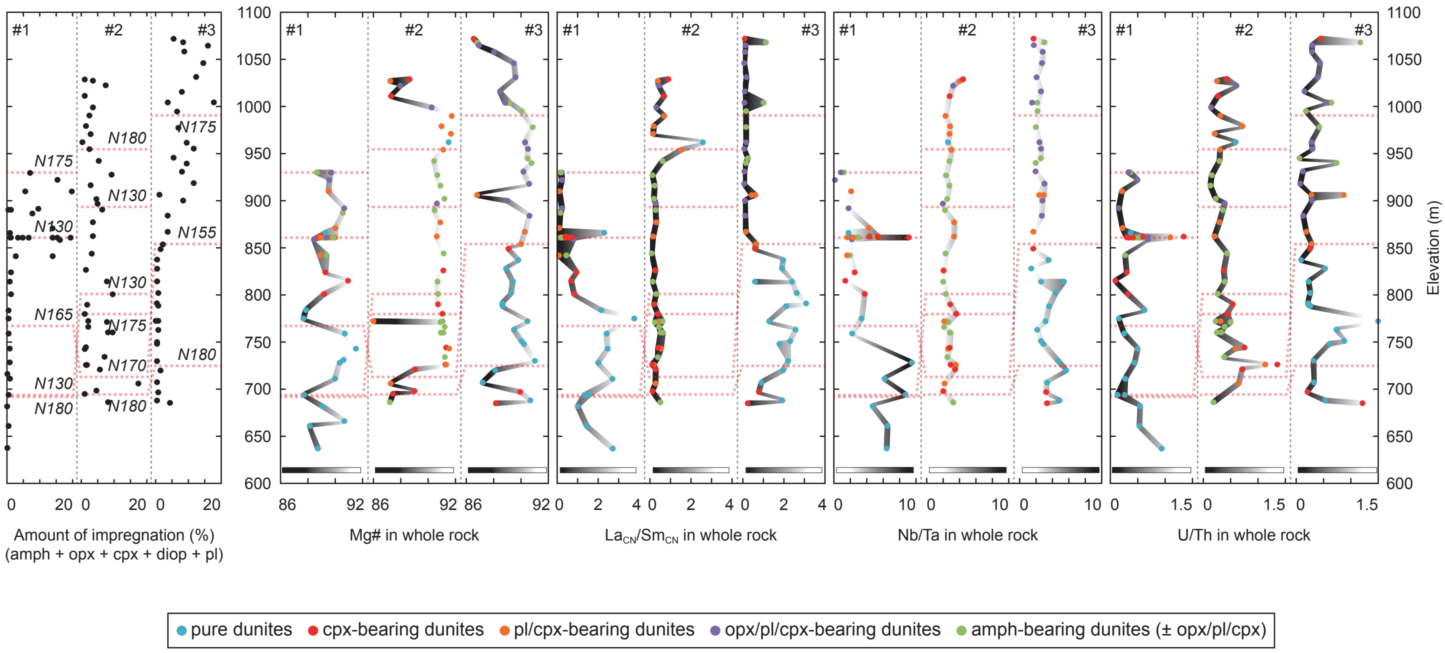

#1
#2
#3
N175
N180
N130
N130
N155
N165
N175
N130
N180
N170
N130
N180
N180
N175
Amount of impregnation (%)
(amph + opx + cpx + diop + pl)
Mg# in whole rock
La_{CN}/Sm_{CN} in whole rock
Nb/Ta in whole rock
U/Th in whole rock
Elevation (m)
pure dunites
cpx-bearing dunites
pl/cpx-bearing dunites
opx/pl/cpx-bearing dunites
amph-bearing dunites (± opx/pl/cpx)

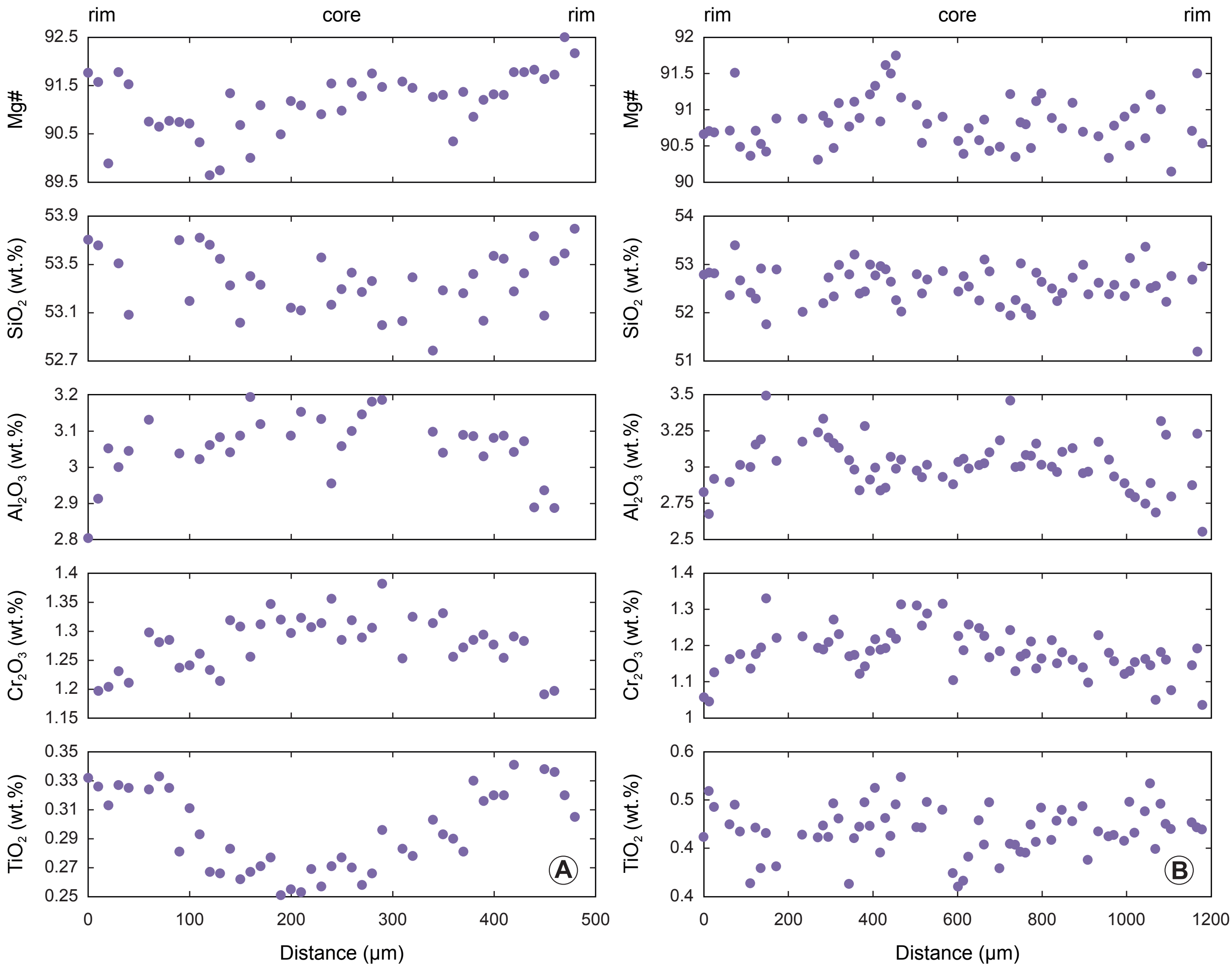

rim
core
rim
Mg#
SiO_2 (wt.%)
Al_2O_3 (wt.%)
Cr_2O_3 (wt.%)
TiO_2 (wt.%)
Distance (μm)
A
B

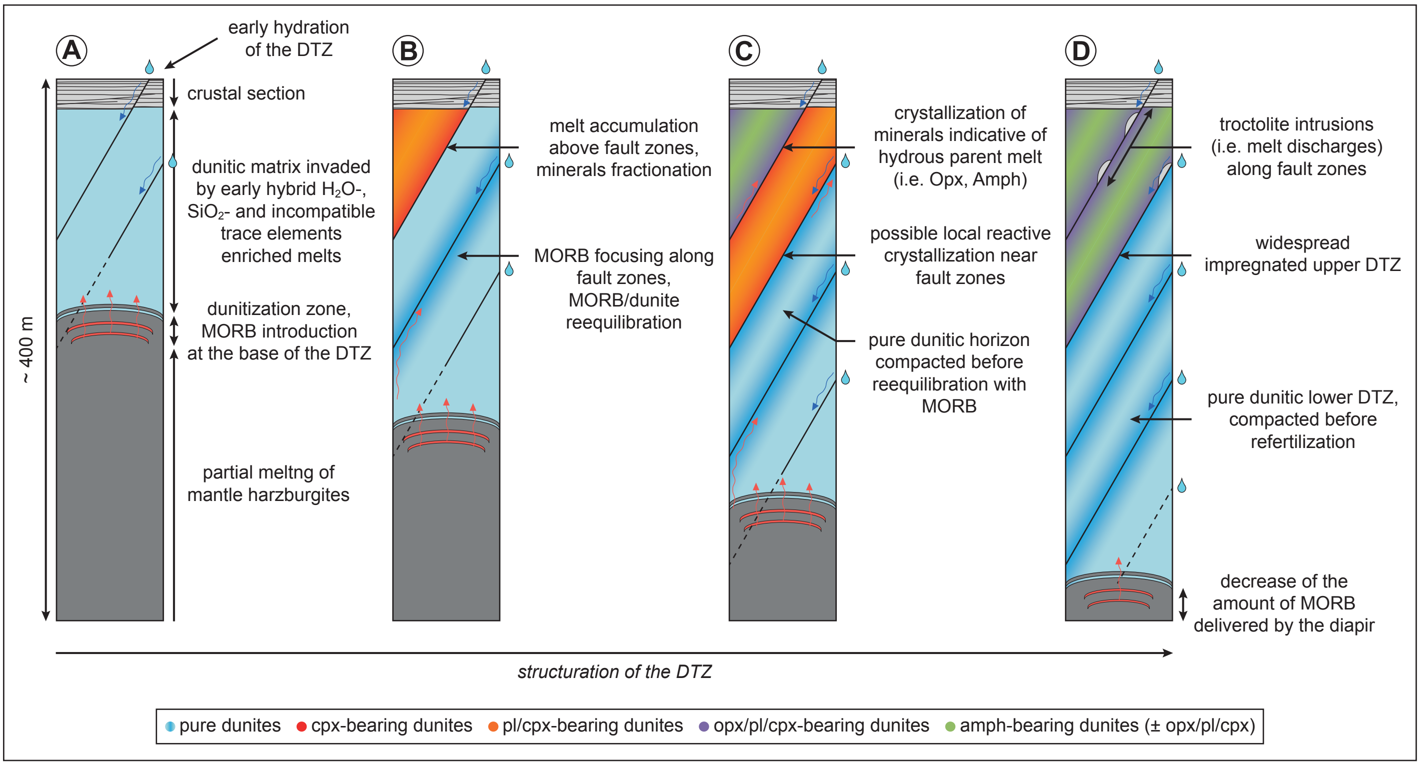
A
early hydration
of the DTZ
crustal section
dunitic matrix invaded
by early hybrid H_2O-,
SiO_2- and incompatible
trace elements
enriched melts
dunitization zone,
MORB introduction
at the base of the DTZ
partial meltng of
mantle harzburgites
~ 400 m
B
melt accumulation
above fault zones,
minerals fractionation
MORB focusing along
fault zones,
MORB/dunite
reequilibration
C
crystallization of
minerals indicative of
hydrous parent melt
(i.e. Opx, Amph)
possible local reactive
crystallization near
fault zones
pure dunitic horizon
compacted before
reequilibration with
MORB
D
troctolite intrusions
(i.e. melt discharges)
along fault zones
widespread
impregnated upper DTZ
pure dunitic lower DTZ,
compacted before
refertilization
decrease of the
amount of MORB
delivered by the diapir
structuration of the DTZ
pure dunites
cpx-bearing dunites
pl/cpx-bearing dunites
opx/pl/cpx-bearing dunites
amph-bearing dunites (± opx/pl/cpx)